Materials & Design 215 (2022) 110412

Contents lists available at ScienceDirect

Materials & Design

journal homepage: www.elsevier.com/locate/matdes

Improvement of acid resistance of Zn-doped dentin by newly generated chemical bonds

Katsuaki Naito [a], Yasutaka Kuwahara [b], Hiroko Yamamoto [a], Yasuhiro Matsuda [c], Katsushi Okuyama [d], Takuya Ishimoto [b], Takayoshi Nakano [b], Hiromi Yamashita [b], Mikako Hayashi [a,*]

[a] Department of Restorative Dentistry and Endodontology, Graduate School of Dentistry, Osaka University, 1-8 Yamada-oka, Suita, Osaka 565-0871, Japan
[b] Division of Materials and Manufacturing Science, Graduate School of Engineering, Osaka University, 2-1 Yamada-oka, Suita, Osaka 565-0871, Japan
[c] Division of Clinical Cariology and Endodontology, Department of Oral Rehabilitation, School of Dentistry, Health Sciences University of Hokkaido, 1757 Kanazawa, Tobetsu-cho, Ishikari-gun, Hokkaido 061-0293, Japan
[d] Department of Dental Materials Sciences, Asahi University School of Dentistry, 1851 Hozumi, Mizuho, Gifu 501-0296, Japan

HIGHLIGHTS

- Zinc, released from bioactive materials, was incorporated into dentin with in approximately 50 μm.
- Zinc-doped dentin demonstrated 30% less acid solubility, helping to improve its anti-carcinogenicity.
- Zinc was incorporated into dentin in a four-fold coordination—, indicating a newly generated covalent bond.
- Quantum beam and synchrotron radiation technologies help in analyzing the bonding states of dentinal elements.

GRAPHICAL ABSTRACT

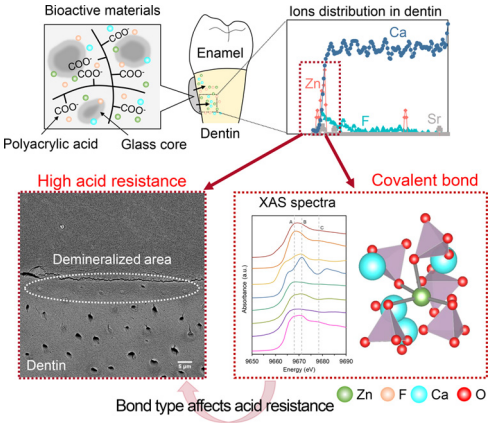

ARTICLE INFO

Article history:
Received 7 September 2021
Revised 18 January 2022
Accepted 18 January 2022
Available online 29 January 2022

Keywords:
Dentin
Dental caries
Chemical state
X-ray absorption spectroscopy
Zinc
Fluoride

ABSTRACT

Dental caries, the world's most prevalent infectious disease, is caused by the diffusion of hydroxyl ions into tooth structures. To prevent dental caries, the application of fluoride (F) and zinc (Zn) ions to teeth surfaces are potential effective measures. In this study, The ionic influence, especially the chemical bond of F and Zn, on the acid resistance of dentin were investigated by particle induced X-ray / gamma-ray emission, X-ray diffraction, X-ray photoelectron spectroscopy and X-ray absorption spectroscopy. The results showed Zn was distributed in the limited surface layer of dentin without altering its crystal structure. From the Zn K edge extended X-ray absorption fine structure, Zn incorporated into dentin was surrounded by oxygen and demonstrated four-fold coordination. The bond length and chemical state of Zn–O in Zn doped dentin suggested newly generated Zn–O covalent bond, which may improve acid resistance of dentin. This study showed that the atomic and molecular structures, such as the molecular distances and chemical state, influenced acid resistance of teeth, emphasizing the validity of chemical state analysis for understanding properties in biomaterials.

* Corresponding author at: Graduate School of Dentistry, Osaka University, 1-8 Yamada-oka, Suita, Osaka 565-0871, Japan.
E-mail address: mikarin@dent.osaka-u.ac.jp (M. Hayashi).

https://doi.org/10.1016/j.matdes.2022.110412
0264-1275/

1. Introduction

Dental caries has been the most common infectious disease in the world for decades. Root caries, which especially occurs on exposed root dentin in elderly people, has become a critical health problem in many developed countries, where societies are aging rapidly [1]. Dental caries demonstrates a complex pathology, showing ion circulation [2]. It is caused by demineralization of the inorganic parts of enamel and dentin by acidic metabolites derived from oral bacteria. On the other hand, the generated ions contribute to remineralization. For these reasons, it is necessary to understand the dynamics of the ions to elucidate the detailed pathophysiology of dental caries.

Dentin is an inorganic–organic composite material surrounded by enamel or cementum. It is composed of an organic part, type I collagen fibers, an inorganic part, hydroxyapatite nanocrystals, and water [3]. Biological apatite (BioHAp), which constitutes dentin and bone, is extremely complex, containing not only hydroxyapatite (HAp, $Ca_{10}(PO_4)_6(OH)_2$), but also diverse calcium phosphate phases, such as octacalcium phosphate (OCP), amorphous calcium phosphate (ACP), and dicalcium phosphate dihydrate [4,5]. Furthermore, HAp in dentin contains vacancies and trace elements, such as carbonate (CO_3^{2-}), magnesium (Mg), fluoride (F), sodium (Na), and zinc (Zn) ions [6–8]. The crystallographic properties promote an impact on complex chemical dynamics in living organisms including HAp crystallinity, demineralization, and remineralization; but how these mechanisms work exactly is still only partly known.

The effect of F on the acid resistance of enamel and dentin has been demonstrated epidemiologically by incorporating F in dentin through toothpaste and water fluoridation [9]. In spite of recent advances in knowledge and clinical practice, dental caries has not been eradicated in developed countries, and in many countries root caries is becoming prevalent and troublesome in elderly people [10]. This suggests that treatment with F alone is not the complete answer to combat dental caries. Further innovative treatments are required to eradicate caries. Recent experiments have proved that combining F with other elements instead of merely using F alone was effective in preventing dental caries [11–14]. In the present study, we focused on incorporating trace elements such as Zn in combination with F. Zn is a group 12 ion with a closed d orbital, and it exhibits similar properties to alkaline earth metals, such as Mg, Ca, and Sr. The roles of Mg and Sr, which are in the same group as Ca, in the inorganic components of dentin have been investigated [14,15]. However, little research has been performed on the effect on the inorganic components, and most studies have only focused on cells and enzymes.

Dental materials have been actively developed with an idea of incorporating various ions into the crystal structures of enamel and dentin with the aim of improving their mechanical and anticariogenic properties. The ion dynamics of these crystal structures have been analyzed by X-ray diffraction (XRD) for the long-range order and by transmission electron microscopy (TEM) [16–18]. These methods offer essential microscopic information of dentin; but important information on ion dynamics needs to be analyzed by the short-range order to identify specific structures at the atomic scale. Recently, analysis of the ion distributions in rodent enamel using atom probe tomography (APT) showed that the effect of F in preventing dental caries is because of substitution of F for Mg–ACP at grain boundaries in enamel HAp [13]. This outcome demonstrated the potential of significantly improving carious prevention by elucidating the ion dynamics at the atomic scale Currently, there are very few researches investigating how chemical bonds form among the constituent elements of dentin or how they may interact to influence dentin properties at the atomic scale. The present study demonstrates a cutting-edge approach to clarify how chemical bonds occur and to identify potentially advantageous ones. The hope is that this research may lead to the design and development of improved dental materials, ultimately radically to change clinical treatments.

The aim of this study is to analyze the ionic influence, especially the chemical bond of Zn, on the acid resistance of dentin using in-air micro-particle induced X-ray and gamma-ray emission (PIXE/PIGE), XRD, X-ray photoelectron spectroscopy, and X-ray absorption spectroscopy (XAS). PIXE/PIGE enables highly sensitive and non-destructive detection of multiple elements by measuring the X-ray fluorescence and gamma rays generated by proton beam collisions [19]. XAS is a method for analyzing the electronic and chemical state. XAS can identify the structure around each constituent element even in amorphous materials, such as glass, and it is highly sensitive to trace elements. Through these methods, the ion dynamics in dentin can be revealed at the atomic scale and the mechanism of the functional expression of F and Zn can be understood. This may allow a move away from the traditional treatment of "drill and fill" to non-drill using a biological approach taking advantages of new understanding of the ion dynamics.

2. Materials and methods

This study was carried out in accordance with protocols approved by the Research Ethics Committee of Osaka University Graduate Schools of Dentistry (H30-E36). Extracted third molars were obtained from participants with the patients' informed consent.

2.1. Consumables

All of the chemicals were of analytical grade and used without further purification. Calcium chloride ($CaCl_2$), zinc fluoride tetrahydrate ($ZnF_2{\cdot}4H_2O$), and zinc phosphate tetrahydrate [$Zn_3(PO_4)_2{\cdot}4H_2O$] were purchased from Fujifilm Wako Pure Chemical (Osaka, Japan). Ammonium phosphate dibasic [$(NH_3)_2HPO_4$], potassium dihydrogen phosphate (KH_2PO_4), potassium hydroxide (KOH), sodium hydroxide (NaOH), zinc nitrate hexahydrate [$Zn(NO_3)_2{\cdot}6H_2O$], zinc oxide (ZnO), zinc carbonate ($ZnCO_3$), strontium carbonate ($SrCO_3$), calcium nitrate tetrahydrate [$Ca(NO_3)_2{\cdot}4H_2O$], 28% ammonium water (NH_3), and acetic acid (CH_3COOH) were purchased from Nacalai Tesque (Kyoto, Japan). Zinc foil was purchased from Nilaco (Tokyo, Japan).

Bioactive glass ionomer (or polyalkenoate) cements (GICs) have been widely used in dental practice for restoring cavities due to dental caries. GICs are composed of fluoro-alumino-silicate glass and polyacrylic acid and harden based on the acid–base reaction. GICs have the characteristic of continuously releasing ions, which contributes to the antimicrobial effect and caries prevention. In this study, three types of GICs were designed to release ions provided by GC (Tokyo, Japan). The composition of each GIC is given in Table 1. ZIF-10 contains two types of fillers: conventional fluoro-alumino-silicate glass and newly developed fluoro-zinc-silicate glass containing Zn, Ca and F as the main components. Fuji VII (Fuji 7) is a typical GIC for protecting dentin, and it has been widely used in the clinic. FRC-02 is a cement in which half of Sr in Fuji 7 is replaced by Ca.

2.2. Preparation of the specimens for PIXE/PIGE

Sample size calculation was performed based on the difference of mineral loss in a pilot study, at α = 5%, with a power of 80%. Assuming an expected mean difference of 2870 mg/cm^3 with a standard deviation of 1700, a minimum of 7 specimens per group was estimated as necessary to identify significant differences

Table 1
Compositions of the materials.

Name	Company		Composition	lot No.
ZIF-10	GC	powder	fluoro-zinc-silicate glass fluoro-alumino-silicate glass	1709251
		liquid	polybasic carboxylic acid polyacrylic acid distilled water	1710200
FRC-02	GC	powder	fluoro-alumino-silicate glass (Sr:Ca = 50:50)	1507161
		liquid	polybasic carboxylic acid polyacrylic acid distilled water	1507161
Fuji VII	GC	powder	fluoro-alumino-silicate glass	1507161
		liquid	polybasic carboxylic acid polyacrylic acid distilled water	1506021

between groups. Considering an inadequacy of the specimens, the final number per group was set on 10.

Ten extracted human third molars stored in saline solution at 4 °C were used in this study. Preparation of the specimens was performed as described previously [20] (Supplemental Fig. 1). In brief, the extracted teeth were perpendicularly cut to the axis at the positions of 0.5 mm above and 7.0 mm below the cement–enamel junction and sectioned into four blocks with a low-speed cutting machine (Isomet, Buehler, IL, USA). The bucco-lingual surfaces were exposed and then covered with one of the three materials (ZIF-10, FRC-02, or Fuji 7). The specimens without the materials served as controls. Consequently, four groups were prepared for the following experiments. The specimens were immersed in 10 ml saline for 3 months at 37 °C so that the released ions were incorporated in the dentin. The solution was substituted with new solution every week. The materials on the specimens were then mechanically removed. These specimens were used for the following experiments.

2.3. In-air micro-PIXE/PIGE measurement

PIXE/PIGE measurement was performed at JAEA Takasaki to obtain the distribution and concentrations of F, Zn, Sr, and Ca in dentin according to a previously reported method [21]. Specimens immersed in saline for 3 months were used. Each block was cut parallel to the longitudinal axis for the exposed root dentin using a diamond wire saw (DWS-3032, Meiwafosis, Tokyo, Japan) to make 500 μm width specimens, which were used as the measurement specimens (Supplemental Fig. 1).

The specimens were bombarded with a 1.7 MeV proton beam in air. The typical beam spot size was approximately 1.0 μm with a beam current of 100 pA. The scanning area was 500 μm long and 250 μm wide. The gamma rays used to measure the F concentration were generated by the $^{19}F(p, \alpha\gamma)^{16}O$ nuclear reaction [22]. The Sr concentration was determined with another detector prepared with a 500 μm X-ray absorber to remove the low-energy X-rays. The gamma-ray yields of reference materials, $Ca_{10}(PO_4)_6(-OH)_{2-2x}F_{2x}$ (x = 0, 0.25, 0.5, 0.75, and 1.0, HOYA Technosurgical, Tokyo, Japan), with similar chemical compounds to those of teeth were also measured. The X-ray yields were also measured for the reference materials mixed with hydroxyapatite and ZnO or $SrCO_3$. The concentrations of Zn and Sr in the reference materials were confirmed by inductively coupled plasma-atomic emission spectrometry (ICP-AES, ICPS-8100, Shimadzu, Kyoto, Japan) before PIXE/PIGE. The PIXE/PIGE data were analyzed with PIXEana1.5 [23].

2.4. Acid resistance test

The acid resistance test was performed to mimic demineralization of dental caries. After PIXE/PIGE, the surfaces of all of the specimens were masked from demineralization with an acid-resistant varnish, except for the exposed root dentin. The residual of the varnish was confirmed on the exposed root dentin surface using a stereomicroscope (SMZ-U, Nikon, Tokyo, Japan). Each specimen was immersed in a 15 ml tube containing 10 ml acid solution (50 mmol/l acetic acid, 2.2 mmol/l $CaCl_2$, 2.2 mmol/l KH_2PO_4, pH 5.0). The specimens were incubated on a shaker at 37 °C for 3 days. The specimens were then washed with deionized water for 30 s and the varnish was mechanically removed from the specimens. Each specimen was stored at 4 °C in 100% humidity until subsequent micro-computed tomography (μCT) analysis.

All of the specimens subjected to PIXE/PIGE were scanned by μCT to investigate the acid resistance of the specimens with applied materials (SMX-100CT, Shimadzu, Kyoto, Japan). The scanning images were collected with 180° rotation of 0.6° per projection step at 35 kV and 200 μA. The data were recorded with 512 × 512 pixel resolution and 10 μm isotropic voxel size. A series of reference phantoms were scanned, which included hydroxyapatite disks with different concentrations (100, 200, 300, and 400 mg/cm^3) and an aluminum pole (1550 mg/cm^3).

Reconstructed images were then created with CT-solver (Shimadzu) and TRI/3D-BON software (Ratoc System Engineering, Tokyo, Japan). We selected a center image from the reconstructed images before and after demineralization and superimposed them on both edges at the crown sides with Image J software (NIH, Bethesda, MD, USA). An overall mineral profile was produced for each specimen. The analysis area used was the same area as PIXE/PIGE analysis. The amount of mineral loss was calculated by integrating the difference of the mineral content profiles of identical specimens before and after demineralization.

2.5. Morphological observation

The specimens after the acid resistance test were dehydrated with ethanol and embedded in epoxy resin and polymerized overnight at 60 °C in a desiccator. The embedded specimens were polished with #600 to #2000 SiC polishing papers. The specimens were further polished with alumina oxide suspensions with diameters of 1.0, 0.3, and 0.05 μm on polishing cloths, and the specimens were then rinsed with distilled water and dried. Au coating was performing to obtain the conductivity with a sputter coater (SC-200, Meiwafosis). Scanning electron microscopy (SEM) obser-

vation was performed with a JSM-F100 scanning electron microscope (JEOL, Tokyo, Japan) operating at 10 keV. Backscattered electron images were taken to detect the dissolved area.

2.6. Synthesis of Zn-doped HAp

Zn-doped HAp was synthesized based on the previous method reported to compare the chemical state with Zn-doped dentin [24]. In brief, 0.1 M $Ca(NO_3)_2{\cdot}4H_2O$, 0.1 M $Zn(NO_3)_2{\cdot}6H_2O$, and 0.06 M $(NH_3)_2HPO_4$ solutions were prepared for synthesis of Zn-doped HAp. The solutions were mixed to achieve the stoichiometric ratio (Ca + Zn)/P = 1.67. The Zn concentration was adjusted to 10 mol% ($Ca_{0.9}Zn_{0.1}(PO_4)_6(OH)_2$). The mixed solution was stirred for 1 h maintaining pH 10 using 28% NH_3 solution. The pH value was continuously monitored with a pH meter (LAQUA F-73, Horiba, Kyoto, Japan) After stirring, the precipitates were filtered under reduced pressure and irrigated with distilled water three times. The precipitates were dried in an oven at 50 °C for 1 day and finally annealed at 500 °C for 4 h. We investigated the stoichiometric (Ca + Zn)/P ratio and crystal properties of Zn-doped HAp by ICP-AES and XRD (Smart Lab, Rigaku, Tokyo, Japan). The stoichiometric (Ca + Zn)/P ratio was 1.59, and Zn-doped HAp was confirmed with HAp formation of a single phase.

2.7. XRD

XRD was performed to investigate whether the incorporated ions affected the crystal structure of dentin. For XRD, we prepared

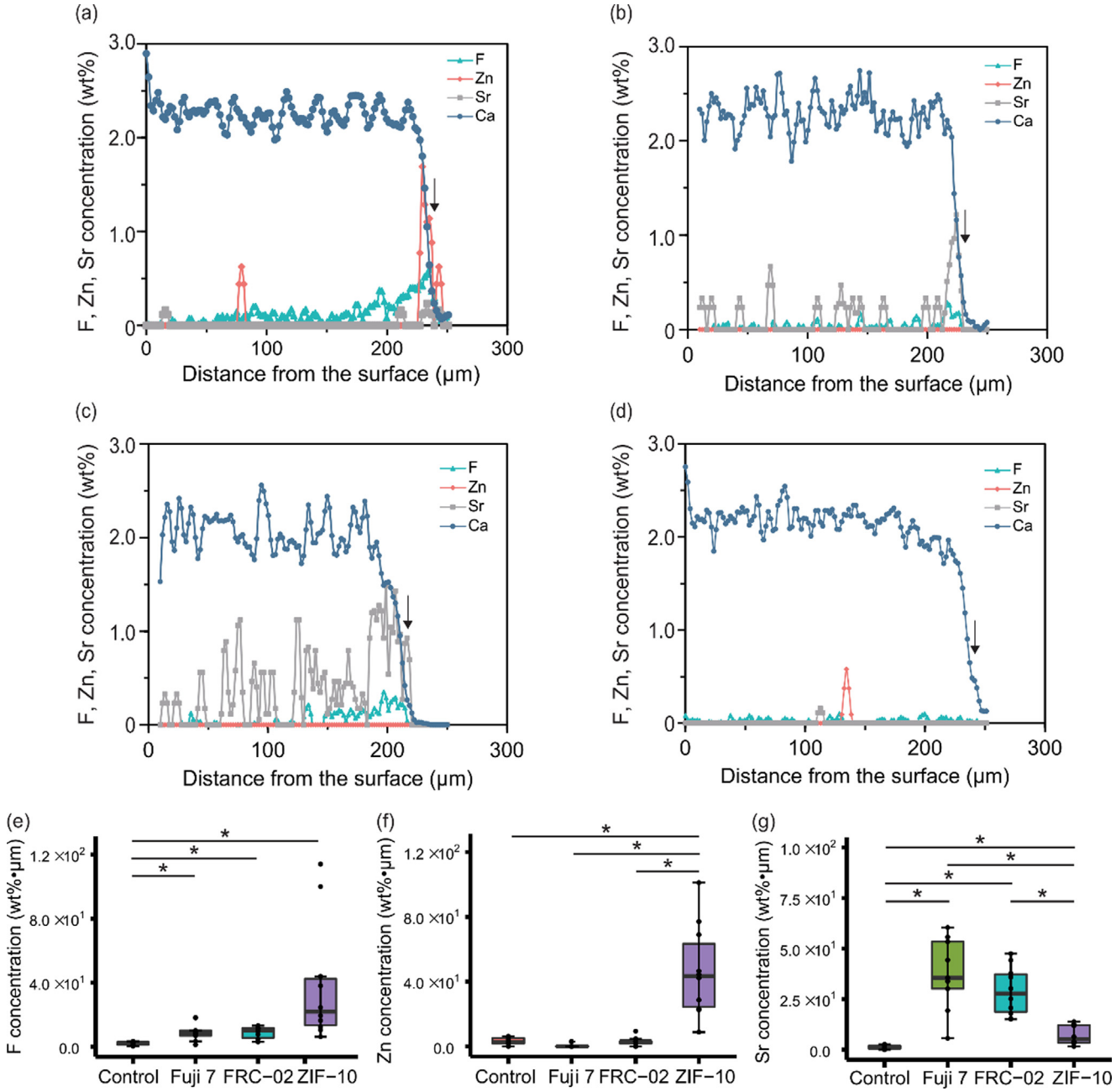

Fig. 1. The PIXE/PIGE spectra of the ion distribution in human dentin: (a) ZIF-10, (b) FRC-02, (c) Fuji 7 and (d) Control. Arrows indicate the surfaces of dentin specimens. A sound surface layer was defined as a position showing 95% of the Ca average concentration in healthy dentin (from 50 to 150 μm). The quantitative analysis with PIXE/PIGE was shown in (e), (f) and (g). These figures show integrated concentration of each ion in the dentin specimens from the surface to 200 μm: (e) F, (f) Zn and (g) Sr, respectively. *: Steel–Dwass test, $p < 0.05$.

Zn-doped dentin, as described in Section 2.2. In brief, human sound third molars (n = 3) were sectioned into four blocks. The exposed root dentin was covered with ZIF-10 and immersed in saline for 1 month to incorporate Zn. The material on the specimens was then mechanically removed. XRD was performed with a Rigaku Smart Lab X-ray diffractometer for the following specimens: Zn-doped dentin, 10 mol% Zn-doped HAp, HAp (Bio-Rad Laboratories, California, USA), Zn foil, ZnO, et $(PO_4)_2{\cdot}4H_2O$, $ZnF_2{\cdot}4H_2O$, $ZnCO_3$, and ZIF-10. The diffraction spectra were recorded in the 2θ range from 10° to 70° using Cu Kα radiation (λ = 1.541 Å, 45 kV, 200 mA) with a step size of 0.02°. The specimens were measured by grazing incidence XRD with a parallel beam where the incident angle was 0.01°.

2.8. X-ray photoelectron spectroscopy

X-ray photoelectron spectroscopy (XPS) was performed with an ESCA-3400 photoelectron spectrometer (Shimadzu) using the Al Kα line to clarify the chemical state of Zn-doped dentin. For XPS, human sound third molars (n = 5) were prepared and cut, as described in Section 2.7. Zn-doped dentin was mechanically scraped from the surface to 50 μm with a surgical knife to obtain powder specimens. The following specimens were prepared for reference: 10 mol% Zn-doped HAp, ZnO, $ZnF_2{\cdot}4H_2O$, $Zn_3(PO_4)_2{\cdot}4H_2O$, and ZIF-10. All of the specimens were placed in an agate mortar and sufficiently crushed, then were attached to the specimen stage on a carbon tape. They were placed in a chamber in which the pressure was maintained at approximately 10^{-6} Pa. Because of charging of the specimens, the binding energy was calibrated using the C 1s photoelectron peak at 284.5 eV [25], which was obtained from carbon tape. The following spectra were recorded: C 1s, O 1s, Zn 2p, and Zn Auger with a step width of 0.05–0.1 eV. All spectra were corrected by subtracting a Shirley method background [26].

2.9. Zn K-edge XAS

The X-ray absorption spectra were recorded in fluorescence mode at the beamline 01B1 station at Spring-8 (JASRI, Harima, Japan). The powder of Zn-doped dentin was obtained as described in Section 2.7. The powder specimens were placed in a stainless steel mold with a diameter 7 mm, and compacted with a pressure of 2 MPa for 5 min to obtain specimens with 1–2 mm thickness. Monochromator energy calibration was performed using ZnO and Zn foil in transmission mode. The fluorescence yield was recorded using a 19-element solid-state detector at room temperature. The data were recorded relative to the Zn K-edge (9660.8 eV) from the 8.0 GeV electron storage ring.

The extended X-ray absorption fine structure (EXAFS) data were analyzed with Athena [27]. The edge energy (E_0) was defined as the maximum of the first derivative of the absorption edge. The edge

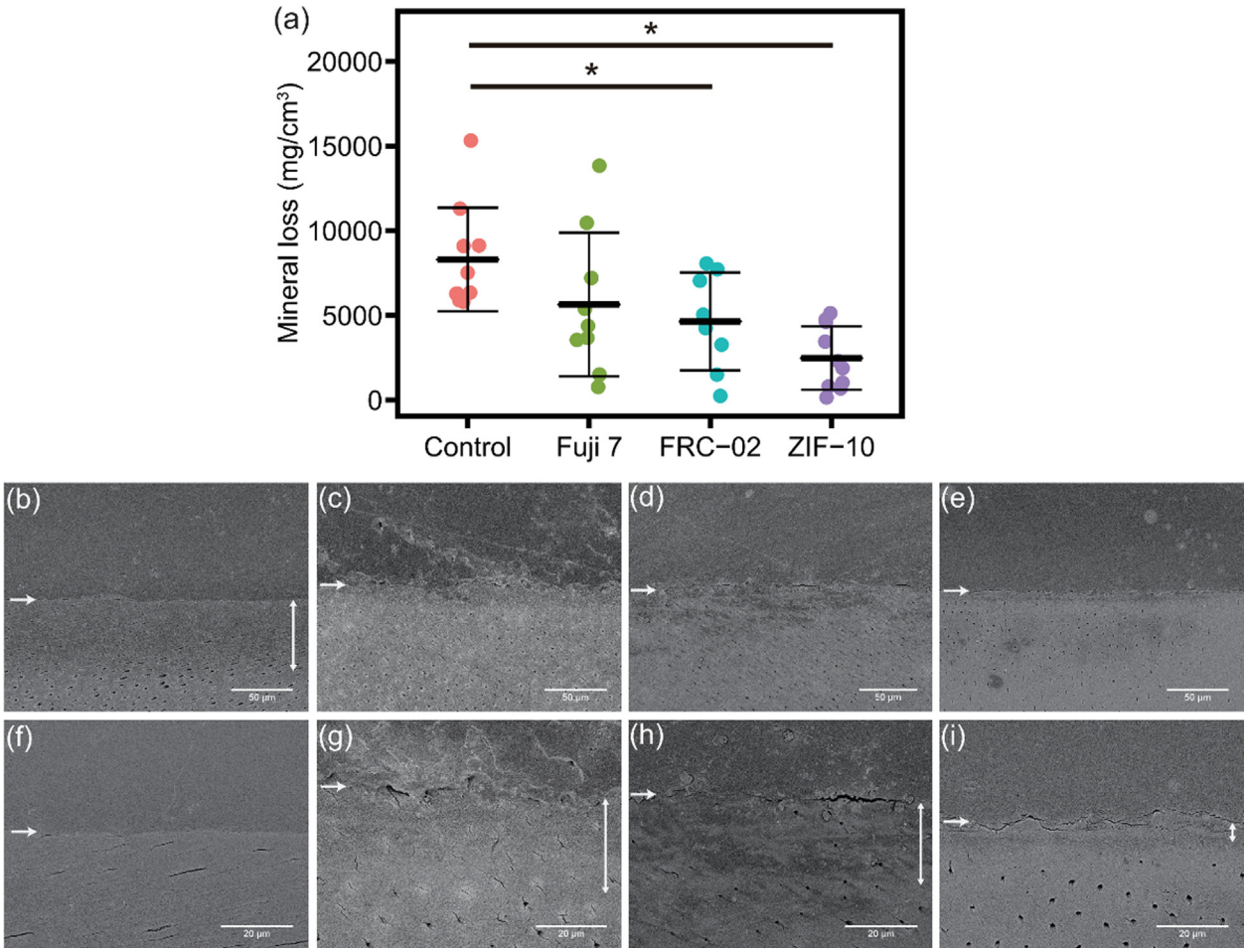

Fig. 2. The acid resistance and SEM images of dentin after the application of ion-release materials. The figure (a) shows the amount of mineral loss in the experimental groups. *: One-way analysis of variance (ANOVA) followed by the post-hoc Tukey honestly significant difference test, $p < 0.05$. The SEM images were shown at low (x500) and high (x1500) magnifications in ZIF-10 (b,f), FRC-02 (c,g), Fuji 7 (d,h), and Control (e,i) groups. The top half of each image is an epoxy resin, and the bottom half is demineralized dentin. A white arrow indicates the top surface of dentin. Double-headed arrow indicates the demineralized area, which demonstrated as dark area compared to the sound dentin. Irregular dentin tubules were observed in the demineralized area.

peaks in the X-ray absorption near edge structure (XANES) regions were normalized for comparison between the specimens and reference materials based on the average absorption coefficient of the spectral region. The $\chi(k)$ function was Fourier transformed using k^3 weighting. Fourier transformation (FT) of the k^3-weighted normalized EXAFS data was performed over the k range 3–12 $Å^{-1}$. Because of the noise signals of the spectra of Zn-doped dentin and Zn-doped HAp, a k range of 3–10 $Å^{-1}$ was selected. The theoretical backscattering paths of the specimens were calculated using FEFF6 [28]. Shell-by-shell fitting was performed in R-space using Artemis [27]. The correction term of the energy (E_0) was allowed to take different values. The amplitude reduction factor (S_0^2) was determined based on the fitting results of Zn foil and ZnO, and it was fixed at S_0^2 = 0.91 when analyzing unknown specimens. In the reference specimens except Zn-doped HAp, the coordination numbers were determined based on the crystal structures determined by XRD. The spectrum of Zn-doped HAp was fitted with a model in which Zn was substituted in the Ca–2 sites of HAp. The model for the Zn-doped dentin spectrum was prepared based on the OCP structure because of the complexity and low crystallinity of dentin [29]. This model was a Zn-containing model with Ca–6 substituted by Zn. The model for ZIF-10 was constructed based on Zn_2SiO_4.

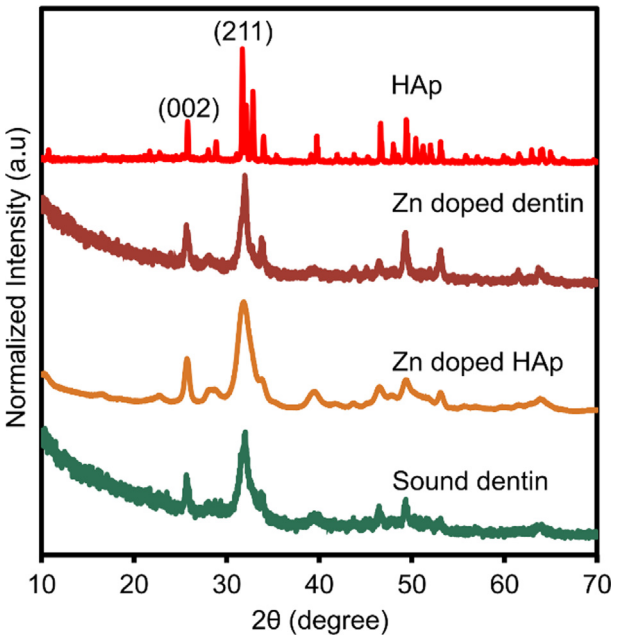

Fig. 3. X-ray diffractograms of Zn-doped dentin and reference specimens. The values of intensity are normalized in order to compare the peak positions of the spectra. The (002) and (211) planes, which are characteristic of HAp, were shown.

2.10. Statistical analysis

The quantitative data obtained by PIXE/PIGE were analyzed by the Steel–Dwass test to compare the materials, while the μCT data were analyzed by one-way analysis of variance (ANOVA) followed by the post-hoc Tukey honestly significant difference test. The significance level was set to $\alpha = 0.05$. The statistical analysis was performed in R (version 3.6.2), and the figures were produced using the ggplot2 package [30,31].

3. Results

3.1. Distributions and concentrations of the ions in dentin

The distributions and concentrations of the ions in each experimental group are shown in Fig. 1. In ZIF-10, Zn was incorporated in the surface layer of dentin within approximately 50 μm (Fig. 1a). Zn was hardly detected in the other groups. F showed

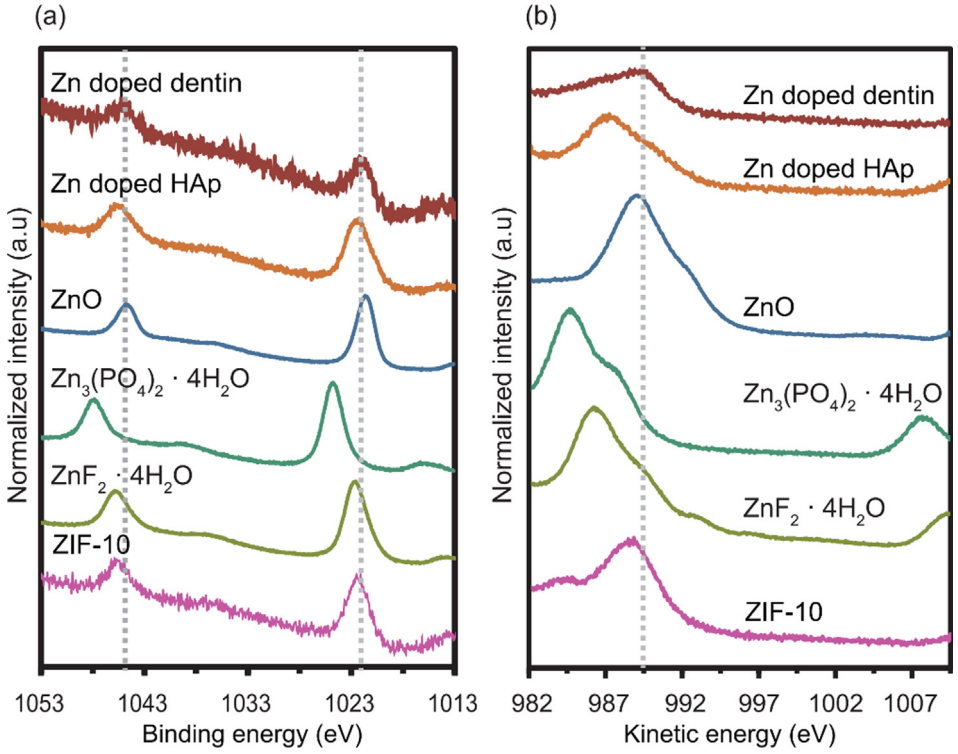

Fig. 4. XPS Zn 2p (a) and Zn Auger (b) spectra. Dotted lines show the peaks of Zn-doped dentin. The values of intensity are normalized in order to compare the peak positions of the spectra.

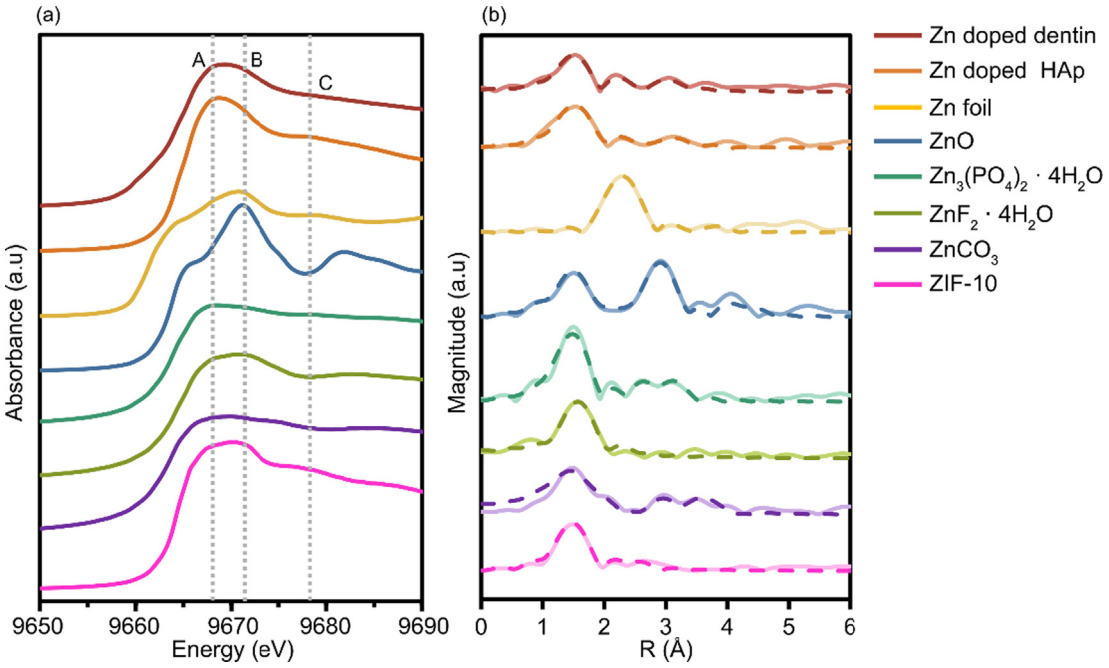

Fig. 5. Zn K-edge XANES (a) and FT-EXAFS (b) spectra of Zn-doped dentin and reference specimens. (a) The spectra are standardized with E0. The dotted lines (A, B and C) were drawn based on the peaks of Zn-doped dentin and HAp in order to compare the spectra. (b) Fourier transform amplitudes (solid lines) and fitting data in R-space (dashed lines).

the highest concentration in the surface layer for all of the materials, and the F concentration gradually decreased moving inwards. In ZIF-10 and Fuji 7, F was discovered in the area around 100 μm from the surface layer. In FRC-02 and Fuji 7, Sr was found relatively deep in dentin. No ions above the background level were detected in the control group.

We evaluated the concentrations of the ions incorporated in dentin for each material (Fig. 1e, f, g). ZIF-10 showed the highest Zn concentration, and significantly more Zn was incorporated in dentin compared with in the other groups ($p < 0.01$) (Fig. 1f). ZIF-10 showed high F concentration, but there was no statistically significant difference compared with the other groups because of large variations (Fig. 1e). FRC-02 and Fuji 7 showed higher Sr concentrations than the other groups (Fig. 1g).

3.2. Acid resistance of dentin as ions were incorporated

Comparison of the amount of mineral loss among the experimental groups is shown in Fig. 2a. ZIF-10 showed the lowest amount of mineral loss. There were significant differences compared with the control group ($p < 0.01$). Among the three F-containing materials, there was no significant difference in mineral loss.

The dissolved root dentin appeared darker in the backscattered electron images when compared with sound dentin (Fig. 2b-i). The surface layer in ZIF-10 showed a limited dissolved area (less than 10 μm). The morphologies of the surfaces were smooth for ZIF-10 and FRC-02; while an irregular and rough surface was observed for Fuji 7. The dissolved areas were up to approximately 30 μm in FRC-02 and Fuji 7; while in the control group, the dissolved area was more than 50 μm. The shape of the dentinal tubules became irregular in the demineralized area in all specimens.

3.3. Analysis of the crystal structure of Zn-doped dentin

The crystallinity of each specimen was evaluated by comparing the half-widths of the XRD spectra (Fig. 3). Zn-doped dentin and Zn-doped HAp showed broad peaks for the (002) and (211) planes. The broad peaks indicate a small crystal size and low crystallinity. ZIF-10 also showed broad peaks with a high background at 10–30° (Supplemental Fig. 2), which indicated that ZIF-10 was an amorphous material, similar to glass. The reference specimens showed sharp peaks, which indicated a homogeneous crystal structure. The crystal structures of the reference specimens were identified by comparing with databases, and these results were used for EXAFS simulation.

3.4. Chemical state of Zn in Zn-doped dentin

The Zn 2p, Zn Auger and O 1s XPS spectra are shown in Fig. 4. The XPS spectrum of Zn-doped dentin showed peaks for Zn $2p_{1/2}$ and Zn $2p_{3/2}$ at binding energies of 1045.2 and 1022.1 eV (Fig. 4a). This spectrum was similar to that of Zn-doped HAp with peaks located at 1045.4 and 1022.3 eV. The peaks of ZnO, $ZnF_2{\cdot}4H_2O$, and ZIF-10 were only slightly different from those of Zn-doped dentin. Since it was difficult to identify the peaks of Zn-doped dentin and reference specimens in Zn 2p spectra, we measured the kinetic energy of the Zn Auger electron to further analyze and understand the chemical states of Zn. The peak of Zn-doped dentin was observed at 988.9 eV (Fig. 4b), which was consistent with ZnO and ZIF-10. Zn-doped HAp showed a slight peak shift to the low energy side compared with Zn-doped dentin, and the peak was observed at 987.3 eV. $ZnPO_4{\cdot}4H_2O$ and $ZnF_2{\cdot}4H_2O$ showed peaks at 984.8 and 986.3 eV, respectively, and these chemical states of Zn were different from those of Zn-doped dentin. Overall, the XPS results indicated that the chemical states of Zn in Zn-doped dentin were similar to those in ZnO and ZIF-10, but slightly different from those in Zn-doped HAp.

3.5. Zn K-edge XANES and EXAFS

The Zn K-edge XANES data for Zn-doped dentin and all of the reference specimens are shown Fig. 5a. Zn-doped dentin showed

Table 2
FT-EXAFS fitting results of Zn-doped dentin and reference specimens.

Specimen	Path	R (Å)	CN	σ^2 (Å)	⊿E (eV)	R-factor
Zn-doped dentin	O1	1.95	3.22	**0.008**	−2.537	3.7%
	P1	2.86	0.80	**0.004**		
	P2	3.47	1.59	**0.003**		
Zn-doped HAp	O1	1.96	4.73	0.011	1.572	2.5%
	P1	2.97	0.40	**0.003**		
	P2	3.54	1.63	**0.004**		
Zn foil	Zn1	2.66	**6**	0.011	4.273	0.3%
	Zn2	2.83	**6**	0.023		
	Zn3	3.92	**6**	0.025		
ZnO	O1	1.97	**4**	0.006	3.191	2.3%
	Zn1	3.29	**6**	0.004		
	Zn2	3.16	**6**	0.005		
	O2	3.77	**9**	0.007		
	Zn3	4.57	**6**	0.007		
$Zn_3(PO_4)_2{\cdot}4H_2O$	O	1.95	**2**	0.011	1.103	1.3%
	P	3.21	**1**	0.020		
	Zn	3.30	**2**	0.017		
$ZnF_2{\cdot}4H_2O$	F	1.81	**2**	0.033	−1.949	2.0%
	O	2.03	**4**	0.014		
$ZnCO_3$	O1	2.01	**6**	0.030	1.132	3.7%
	C	3.01	**6**	0.014		
	O2	3.16	**6**	0.016		
	Zn	3.92	**6**	0.012		
	O3	4.07	**6**	**0.003**		
ZIF-10	O	1.94	**4**	0.008	0.929	2.6%
	Si	3.08	**2**	0.015		

Amplitude reduction factor 0.91 was determined based on the fitting results from Zn foil and ZnO. The coordination number was basically defined from the crystal structure, as shown bold fonts. For unknown specimens (Zn-doped dentin), Debye-Waller factors were fixed at optimal values due to the influence of multiple close by shells were present (bold fonts at σ^2). ΔE represents the correction term between the measured value of the absorption edge and the theoretical value of E_0.

a broad peak from 9668 to 9671 eV, indicated by the dashed lines A and B. The spectrum of Zn-doped HAp showed similarities with the spectrum of Zn-doped dentin, but it differed in that it contained a slight auxiliary peak at 9678 eV. ZnO showed a sharp peak at dashed line B, while ZIF-10 only exhibited a broad peak from 9667 to 9672 eV, indicating a clear difference from the other specimens. $ZnCO_3$ exhibited a small shoulder peak at 9675 eV, which was different from $ZnF_2{\cdot}4H_2O$ with the same coordination environment. No pre-edge peaks were found for any of the specimens.

The Zn K-edge EXAFS data and results of the fitting simulations are shown in Fig. 5b and Table 2. The Zn k^3-weighted EXAFS oscillation spectra are shown in Fig. 5a. The peaks at the first shell were consistent, except for Zn foil. These results showed the Zn–O bond according to simulated data. The bond length of Zn–O in Zn-doped dentin was 1.95 Å. Zn-doped HAp, ZnO, $Zn_3(PO_4)_2{\cdot}4H_2O$, and ZIF-10 showed approximate Zn–O bond lengths of 1.96, 1.97, and 1.95 Å, respectively. For $ZnF_2{\cdot}4H_2O$ and $ZnCO_3$ with octahedral coordination, the Zn–O bond lengths were noticeably longer (2.03 and 2.01 Å). The second coordination shell of Zn-doped dentin representing Zn–P had a bond length of 2.86 Å. Compared with Zn-doped dentin, Zn–P in Zn-doped HAp and $Zn_3(PO_4)_2{\cdot}4H_2O$ showed longer bond lengths of 2.97 and 3.26 Å.

4. Discussion

4.1. Distribution of the ions in dentin

We found the following three features in the distributions of the ions (F, Zn and, Sr) in dentin: F showed the highest concentration in the surface layer but decreased towards the inner layer; Zn was distributed in the surface layer up to 50 μm deep; Sr was found with relatively high concentration in the deep layer (>100 μm deep).

In the ZIF-10 group, Zn was detected at approximately 80 and 230 μm depth in the PIXE/PIGE spectra. The peak in the surface layer at 230 μm suggested that Zn released from materials and incorporated into dentin; while the peaks at 80 μm in ZIF-10 group and at 130 μm in the control group were assumed to be the inherent zinc delivered from dentin. Healthy dentin contained 80–180 ppm of Zn [32,33], which played a role as an activator of matrix metalloproteinases [34]. In other study, Zn was also detected around pulp chamber in dentin [35]. These findings support the inherent Zn peak in the deep area observed in the present study.

There are two possible mechanisms of how ions penetrate and incorporate in dentin: diffusion in the solids based on Fick's diffusion equation; or diffusion through dentinal tubules, which are dentinal microstructures with an internal diameter of approximately 1–5 μm. F concentrations tended to decrease with distance from the materials from which ions were released, suggesting solid diffusion in accordance with Fick's diffusion equation. It is also possible to diffuse ions through dentinal tubules containing intratubular fluid, which has a composition similar to that of interstitial fluid and contributes to mineralization and ion exchange [36]. Because dentinal tubules were intentionally exposed when preparing the specimens, the ions released from the materials could penetrate into the tubules [19].

The Zn diffusion pattern differed from those of F and Sr. Zn was distributed in the limited surface layer of dentin, suggesting that Zn could not diffuse into the deep part of dentin. Originally, Zn is difficult to incorporate in HAp. As the Zn concentration in HAp increases, the crystal size and crystallinity of HAp significantly decrease [37,38]. This phenomenon can be explained by the difference in the ionic radii and coordination numbers of Zn (0.74 Å) and Ca (0.99 Å). When Zn was substituted for Ca in HAp, structural irregularity and breakdown of the apatite structure were induced by differences in the ionic radii [39]. This may be why Zn could not diffuse in dentin. It is also possible that precipitation of Zn_3(-

$PO_4)_2{\cdot}4H_2O$ by incorporating Zn affects the crystallinity of HAp [40,41]. The XRD spectrum of Zn-doped dentin did not show any peaks derived from zinc phosphate or similar compounds, indicating that precipitation of other crystals did not occur.

4.2. Effect of Zn incorporation on the apatite structure in dentin

The spectrum of Zn-doped dentin showed a similar shape to that of Zn-doped HAp and broad peaks for the (002) and (211) planes (Fig. 3), suggesting low crystallinity owing to the amorphous phase. Even in the surface layer, which demonstrated the highest concentrations of multiple ions, the spectrum of Zn-doped dentin did not differ from that of sound dentin, suggesting that the ions were incorporated in the crystal lattice and did not significantly affect the crystal structure.

4.3. Analysis of the short-range order of Zn in dentin

Zn can have four-, five-, six-, and eight-fold coordination [42]. ZnO has four-fold coordination with each Zn atom tetrahedrally coordinated to four O atoms. ZIF-10 is a glass material with a SiO_4^{2-} network, where the XRD spectrum shows amorphous phases. Zn in ZIF-10 is considered to have four-fold coordination in the SiO_4^{2-} network, because it has been reported from XANEs analysis of Zn-containing glasses and Zn-loaded zeolite that Zn in the SiO_4^{2-} network has the same structure [43,44]. Hence, we used Zn_2SiO_4 with Si–O–Zn and four-fold coordination in the glass framework as the analysis model of the short-range order. Regarding incorporation of Zn in HAp, Matsunaga *et al.* found that Zn-doped HAp is incorporated with five-fold coordination by XANES and density functional theory (DFT) calculations [24]. Tang *et al.* proposed that the state of Zn is maintained in four-fold coordination by O atoms by XANES and EXAFS analysis [45]. Zn-doped HAp showed different binding energies for ZnO and ZIF-10 by XPS and XANES. Moreover, because the coordination number of Zn-doped HAp was 4.73 from FT-EXAFS fitting (Table 2), it was estimated that Zn in Zn-doped HAp had five-fold coordination.

The binding energy of Zn-doped dentin was close to those of ZnO and ZIF-10 with four-fold coordination (Fig. 4). This was similar in the XANES spectra, in which there was a broad peak at 9668–9672 eV. Takatsuka *et al.* analyzed the local structure of Zn in dentin using XAS data, but no detailed structural analysis was performed [46]. The first and second coordination shells in Zn-doped dentin were found to be O and P atoms, respectively, and the coordination number of Zn–O was 3.22 from the results of FT-EXAFS fitting (Fig. 5b and Table 2). Because the minimum coordination number of Zn is four, as mentioned above, we estimated that the coordination number of Zn in Zn-doped dentin was four. The coordination number obtained by EXAFS was smaller than the theoretical value of four. It is presumed that the error between the theoretical and measured values is because of the heterogeneity of the specimens and the use of the fluorescence method for XAS [47]. Therefore, we estimated the coordination numbers of Zn-doped dentin using FT-EXAFS fitting in combination with comparing XPS and XANES spectra which were obtained from reference specimens, because determination of the coordination number by FT-EXAFS fitting may cause some errors. As a result, the coordination numbers calculated by FT-EXAFS did not show significant differences from those of the reference specimens.

Regarding the mechanism of incorporating trace elements in dentin, we considered two hypotheses: substitution for Ca near a vacancy and substitution for Ca in amorphous phases, such as ACP and OCP. BioHAp is a non-stoichiometric material and contains vacancies in the crystal lattice, which are involved in substitution with foreign ions [6]. The detailed mechanism of incorporating Zn in HAp has been demonstrated by experimental and theoretical XANES results, where the Ca^{2+} vacancy-defect complex is present near Zn and plays an important role in Zn substitution in HAp [24]. The XPS results showed that Zn had different environments in Zn-doped dentin and Zn-doped HAp because of the different binding energies. When analyzing Zn-doped dentin by FT-EXAFS fitting, we used the same HAp model as the fitting model for Zn-doped HAp, but we were unable to fit the spectrum. FT-EXAFS fitting showed differences in the coordination numbers, indicating that the mechanism of incorporating Zn in dentin was different from that of Zn-doped HAp. The OCP model with Zn incorporated in Ca–6 sites has been prepared as the model for FT-EXAFS fitting of Zn-doped dentin [29]. According to the results obtained from DFT, this model has the smallest formation energies for substitution of Zn at Ca–6 sites. Because Zn^{2+} has a smaller radius than Ca^{2+}, the coordination number of Zn decreases when incorporated in OCP, preferring four-fold coordination. We were able to fit the FT-EXAFS of Zn-doped dentin using the spectrum of the Ca–6 substitution model in OCP. Although the presence of OCP in dentin has been reported [5], its location remains unclear. OCP has a similar structure to HAp, and it has a hydration layer, leading to high chemical activity. Therefore, it is possible that it contributed to substitution with Zn. In summary, incorporation of Zn in dentin is suggested to occur by substitution of Ca in OCP rather than by substitution of Ca near vacancies.

It is also possible that Zn incorporated in dentin not only with the ionic state of the released materials, but also while maintaining the local structure of Zn in ZIF-10. The GIC, which is the main component of ZIF-10, has a SiO_4^{2-} network with cations such as Al and Ca, which is formed by Si–O to cation cross-linking [48,49]. The results of XPS and XANES showed that the chemical state of Zn were similar to those of ZIF-10, suggesting that Zn maintained a state like a cluster species bound to O and Si. This Si–O–Zn cluster may be incorporated in the voids or cavities of dentin.

In this study, we were able to determine the local structure around Zn, but we were unable to analyze the middle-range order around the substitution sites. This is the reason why the crystallographic structure in dentin is still unclear. No link has been made between the crystal structure and the information about dentin, such as association of collagen fibers and non-collagenous dentin protein with inorganic materials and localization of ACP and OCP. Therefore, there is insufficient information to prove the hypothesis, and further research is needed.

4.4. Mechanism of improvement of the acid resistance of dentin by incorporating Zn

Mineral loss decreased in the dentin with F or Zn incorporated (Fig. 2), suggesting that not only F, but also Zn contributed to improving the acid resistance. The reason for the positive effect of Zn can be explained by the difference of chemical state between Zn–O and Ca–O bonds in dentin. In general, a difference of the chemical state in crystals depends on the electronegativity of the constituent elements. The larger the difference in the electronegativity between the elements involved in the bonding, the higher the degree of ionic bonding. While, as the difference in electronegativity decreases, the ratio of covalent bond increases. The ionic radius and the shape of the orbitals in the covalent bonds are closely related to the coordination number, which is a factor in determining the chemical state.

Ca–O bonds, which influence the solubility of HAp, have weak binding energy and are mostly ionized as Ca^{2+} [50]. Since the electronegativity of Zn is higher than that of Ca, Zn–O bonds were inevitably increased in the ratio of covalent bonds. Previous study showed that OCP incorporated Zn, which was assumed to be Bio-

HAp, was increased the binding energy by forming covalent bonds [29]. The Zn–O bond has four-fold coordination, which is inferred to be sp^3 hybrid orbitals, showing the characteristics of covalent bonds. Thus, the incorporation of Zn increased Zn–O bonds having the ratio of covalent bonds compared to Ca–O bonds. This may be why the acid resistance of dentin improves when Zn is incorporated in dentin.

Introducing Zn in dentin may compensate for lattice defects in HAp. Research has suggested that introducing Zn in carbonate apatite, which resembles BioHAp, reduces the lattice defects and improves the acid resistance [51,52]. Lattice strain and defects lead to inferior chemical stability, which decreases the acid resistance. Dentin partially forms carbonic apatite and has defects in the crystal lattice because it contains approximately 5 wt% CO_3^{2-} [8]. Therefore, the chemical penetration and incorporation of Zn in dentin reduced the lattice defects and contributed to improve the acid resistance.

The improvement of the acid resistance could also be caused by higher concentration of F or Zn. In fluoride, there was no significant correlation between the F penetration and Ca loss. This suggested that the surface density of F is critical rather than its penetration depth into dentin [20]. The high-zinc apatite showed a clear correlation between zinc substitution level and stiffness and hardness [53]. Since it is not easy to accurately and quantitatively measure the concentration of in enamel and dentin, their relationship to acid resistance is still unclear. Therefore it is necessary to clarify the role of each ion in the future.

We could not examine the effect of Zn alone in this study, because multiple ions were released from the restorative materials. However, the results from μCT and SEM observation, plus previous theoretical reports, strongly suggest that Zn significantly contributes to improve the acid resistance of dentin.

5. Conclusions

We demonstrated multi-scale analyses to understand how multiple ions penetrated and incorporated in dentin and influenced its acid resistance. We focused on the role of Zn, which has closed d orbitals. Zn was penetrated and incorporated in the limited surface layer of dentin without any alteration to the dentin crystal structure. The binding energy of Zn in Zn-doped dentin was comparable with those in ZnO and ZIF-10. The results of FT-EXAFS showed that Zn demonstrated four-fold coordination. The bond length and chemical state of Zn–O in Zn-doped dentin suggested newly generated Zn–O covalent bond. This may be why the acid resistance of dentin improves when Zn and F are incorporated in dentin rather than F alone.

The comprehensive analyses using PIXE/PIGE, XRD, XPS and XAS enabled to elucidate the ionic dynamics in dentin at the atom-scale. Those clarified the atomic and molecular structures, such as molecular distances and chemical bonds, influenced on the macroscopic acid resistance of dentin. The combination of the atom-scale and theoretical analyses on the ionic performance in dentin helped with deep understanding of the dynamics of dental caries. These analyses also help with suggesting how to design and develop future dental materials for caries preventions. This will encourage the biological minimal intervention approach in treating dental caries rather than traditional "drill and fill".

Data availability

The raw data required to reproduce these findings can be obtained by contacting the corresponding author.

Declaration of Competing Interest

The authors declare that they have no known competing financial interests or personal relationships that could have appeared to influence the work reported in this paper.

Acknowledgments

This study was supported by Grants-in-Aid for Scientific Research (17H04382, 17K11705, and 20H00552) from the Japan Society for the Promotion of Science. In-air micro-PIXE/PIGE measurement was performed at Takasaki Ion Accelerators for Advanced Radiation Application. XAS was performed at SPring-8 (2019B1091 and 2019B1114). We thank the staff of the QST Takasaki group and the staff of JASRI for their support with the experiments.

Appendix A. Supplementary material

Supplementary data to this article can be found online at https://doi.org/10.1016/j.matdes.2022.110412.

References

[1] R.J. Wierichs, H. Meyer-Lueckel, Systematic review on noninvasive treatment of root caries lesions, J. Dent. Res. 94 (2) (2015) 261–271, https://doi.org/10.1177/0022034514557330.
[2] N.B. Pitts, D.T. Zero, P.D. Marsh, K. Ekstrand, J.A. Weintraub, F. Ramos-Gomez, J. Tagami, S. Twetman, G. Tsakos, A. Ismail, Dental caries, Nat. Rev. Dis. Prim. 3 (2017) 17030, https://doi.org/10.1038/nrdp.2017.30.
[3] A. Linde, M. Goldberg, Dentinogenesis, Crit. Rev. Oral Biol. Med. 4 (5) (1993) 679–728, https://doi.org/10.1177/10454411930040050301.
[4] P. Houllé, J.C. Voegel, P. Schultz, P. Steuer, F.J.G. Cuisinier, High Resolution Electron Microscopy: Structure and growth mechanisms of human dentin crystals, J. Dent. Res. 76 (1997) 895–904, https://doi.org/10.1177/00220345970760041101.
[5] P. Bodier-Houllé, P. Steuer, J.-C. Voegel, F.J.G. Cuisinier, First experimental evidence for human dentine crystal formation involving conversion of octacalcium phosphate to hydroxyapatite, Acta Crystallogr. Sect. D Biol. Crystallogr. 54 (6) (1998) 1377–1381.
[6] R.A. Young, S. Spooner, Neutron diffraction studies of human tooth enamel, Arch. Oral Biol. 15 (1) (1970) 47–63, https://doi.org/10.1016/0003-9969(70)90144-5.
[7] N.L. Derise, S.J. Ritchey, Mineral composition of normal human enamel and dentin and the relation of composition to dental caries: II. Microminerals, J. Dent. Res. 53 (4) (1974) 853–858, https://doi.org/10.1177/00220345740530041601.
[8] R. Zapanta LeGeros, Apatites in biological systems, Prog. Cryst. Growth Charact. 4 (1-2) (1981) 1–45.
[9] H.P. Whelton, A.J. Spencer, L.G. Do, A.J. Rugg-Gunn, Fluoride revolution and dental caries: Evolution of policies for global use, J. Dent. Res. 98 (2019) 837–846, https://doi.org/10.1177/0022034519843495.
[10] W. Marcenes, N.J. Kassebaum, E. Bernabé, A. Flaxman, M. Naghavi, A. Lopez, C.J. L. Murray, Global burden of oral conditions in 1990–2010: A systematic analysis, J. Dent. Res. 92 (2013) 592–597, https://doi.org/10.1177/0022034513490168.
[11] C. González-Cabezas, C.E. Fernández, Recent advances in remineralization therapies for caries lesions, Adv. Dent. Res. 29 (1) (2018) 55–59, https://doi.org/10.1177/0022034517740124.
[12] A. Lussi, T.S. Carvalho, The future of fluorides and other protective agents in erosion prevention, Caries Res. 49 (Suppl. 1) (2015) 18–29, https://doi.org/10.1159/000380886.
[13] L.M. Gordon, M.J. Cohen, K.W. MacRenaris, J.D. Pasteris, T. Seda, D. Joester, Amorphous intergranular phases control the properties of rodent tooth enamel, Science (80-.) 347 (6223) (2015) 746–750.
[14] F. Lippert, A.T. Hara, Strontium and caries: A long and complicated relationship, Caries Res. 47 (2013) 34–49, https://doi.org/10.1159/000343008.
[15] H.P. Wiesmann, T. Tkotz, U. Joos, K. Zierold, U. Stratmann, T. Szuwart, U. Plate, H.J. Höhling, Magnesium in newly formed mineral of rat incisor, J. Bone Miner. Res. 12 (1997) 380–383, https://doi.org/10.1359/jbmr.1997.12.3.380.
[16] J. Xue, A.V. Zavgorodniy, B.J. Kennedy, M.V. Swain, W. Li, X-ray microdiffraction, TEM characterization and texture analysis of human dentin and enamel, J. Microsc. 251 (2) (2013) 144–153, https://doi.org/10.1111/jmi.12053.
[17] J.C. Voegel, R.M. Frank, Ultrastructural study of apatite crystal dissolution in human dentine and bone, J. Biol. Buccale. 5 (1977) 181–194.
[18] C. Besnard, R.A. Harper, E. Salvati, T.E.J. Moxham, L. Romano Brandt, G. Landini, R.M. Shelton, A.M. Korsunsky, Analysis of in vitro demineralised human

enamel using multi-scale correlative optical and scanning electron microscopy, and high-resolution synchrotron wide-angle X-ray scattering, Mater. Des. 206 (2021) 109739, https://doi.org/10.1016/j.matdes.2021.109739.
[19] H. Yamamoto, Y. Iwami, T. Unezaki, Y. Tomii, S. Ebisu, Fluoride uptake in human teeth from fluoride-releasing restorative material in vivo and in vitro: Two-dimensional mapping by EPMA-WDX, Caries Res. 35 (2001) 111–115, https://doi.org/10.1159/000047441.
[20] K. Yagi, H. Yamamoto, R. Uemura, Y. Matsuda, K. Okuyama, T. Ishimoto, T. Nakano, M. Hayashi, Use of PIXE/PIGE for sequential Ca and F measurements in root carious model, Sci. Rep. 7 (2017) 13450, https://doi.org/10.1038/s41598-017-14041-4.
[21] H. Yamamoto, M. Nomachi, K. Yasuda, Y. Iwami, S. Ebisu, N. Yamamoto, T. Sakai, T. Kamiya, Fluorine mapping of teeth treated with fluorine-releasing compound using PIGE, Nucl. Instruments Methods Phys. Res. Sect. B Beam Interact. Mater. Atoms. 210 (2003) 388–394. 10.1016/S0168-583X(03)01039-5.
[22] S.O.F. Dababneh, K. Toukan, I. Khubeis, Excitation function of the nuclear reaction $^{19}F(p, \alpha\gamma)^{16}O$ in the proton energy range 0.3–3.0 MeV, Nucl. Instruments Methods Phys. Res. Sect. B Beam Interact. Mater. Atoms. 83 (3) (1993) 319–324, https://doi.org/10.1016/0168-583X(93)95849-Z.
[23] T. Sakai, T. Kamiya, M. Oikawa, T. Sato, A. Tanaka, K. Ishii, JAERI Takasaki in-air micro-PIXE system for various applications, Nucl. Instruments Methods Phys. Res. Sect. B Beam Interact. Mater. Atoms. 190 (1-4) (2002) 271–275, https://doi.org/10.1016/S0168-583X(02)00469-X.
[24] K. Matsunaga, H. Murata, T. Mizoguchi, A. Nakahira, Atsushi Nakahira, Mechanism of incorporation of zinc into hydroxyapatite, Acta Biomater. 6 (6) (2010) 2289–2293, https://doi.org/10.1016/j.actbio.2009.11.029.
[25] Y. Kuwahara, Y. Yoshimura, K. Haematsu, H. Yamashita, Mild deoxygenation of sulfoxides over plasmonic molybdenum oxide hybrid with dramatic activity enhancement under visible light, J. Am. Chem. Soc. 140 (29) (2018) 9203–9210, https://doi.org/10.1021/jacs.8b0471110.1021/jacs.8b04711.s001.
[26] D.A. Shirley, High-resolution x-ray photoemission spectrum of the valence bands of gold, Phys. Rev. B. 5 (12) (1972) 4709–4714, https://doi.org/10.1103/PhysRevB.5.4709.
[27] B. Ravel, M. Newville, ATHENA, ARTEMIS, HEPHAESTUS: data analysis for X-ray absorption spectroscopy using IFEFFIT, J. Synchrotron Radiat. 12 (2005) 537–541, https://doi.org/10.1107/S0909049505012719.
[28] J.J. Rehr, R.C. Albers, Theoretical approaches to x-ray absorption fine structure, Rev. Mod. Phys. 72 (3) (2000) 621–654, https://doi.org/10.1103/RevModPhys.72.621.
[29] K. Matsunaga, First-principles study of substitutional magnesium and zinc in hydroxyapatite and octacalcium phosphate, J. Chem. Phys. 128 (2008), https://doi.org/10.1063/1.2940337.
[30] R Core Team, R: A language and environment for statistical computing, 2019. https://www.r-project.org/.
[31] H. Wickham, ggplot2: Elegant graphics for data Analysis, Springer-Verlag, New York, 2016. https://ggplot2.tidyverse.org.
[32] E.L. Lakomaa, I. Rytömaa, Mineral composition of enamel and dentin of primary and permanent teeth in Finland, Scand. J. Dent. Res. 85 (1977) 89–95, https://doi.org/10.1111/j.1600-0722.1977.tb00537.x.
[33] N. Charadram, C. Austin, P. Trimby, M. Simonian, M.V. Swain, N. Hunter, Structural analysis of reactionary dentin formed in response to polymicrobial invasion, J. Struct. Biol. 181 (3) (2013) 207–222.
[34] E. Morgunova, A. Tuuttila, U. Bergmann, M. Isupov, Y. Lindqvist, G. Schneider, K. Tryggvason, Structure of Human Pro-Matrix Metalloproteinase-2: Activation Mechanism Revealed, Science (80-.) 284 (5420) (1999) 1667–1670.
[35] R.M. Sulyanto, M. Kang, S. Srirangapatanam, M. Berger, F. Candamo, Y. Wang, J. R. Dickson, M.W. Ng, S.P. Ho, Biomineralization of dental tissues treated with silver diamine fluoride, J. Dent. Res. 100 (10) (2021) 1099–1108, https://doi.org/10.1177/00220345211026838.
[36] C.T. Coffey, M.J. Ingram, A.M. Bjorndal, Analysis of human dentinal fluid, Oral Surgery, Oral Med. Oral Pathol. 30 (6) (1970) 835–837, https://doi.org/10.1016/0030-4220(70)90348-8.
[37] F. Miyaji, Y. Kono, Y. Suyama, Formation and structure of zinc-substituted calcium hydroxyapatite, Mater. Res. Bull. 40 (2) (2005) 209–220, https://doi.org/10.1016/j.materresbull.2004.10.020.
[38] F. Ren, R. Xin, X. Ge, Y. Leng, Characterization and structural analysis of zinc-substituted hydroxyapatites, Acta Biomater. 5 (8) (2009) 3141–3149, https://doi.org/10.1016/j.actbio.2009.04.014.
[39] A. Bigi, E. Foresti, M. Gandolfi, M. Gazzano, N. Roveri, Isomorphous substitutions in β-tricalcium phosphate: The different effects of zinc and strontium, J. Inorg. Biochem. 66 (1997) 259–265, https://doi.org/10.1016/S0162-0134(96)00219-X.
[40] X. Zhao, Y. Zhu, Z. Zhu, Y. Liang, Y. Niu, J. Lin, Characterization, dissolution, and solubility of Zn-substituted hydroxylapatites $[(Zn_xCa_{1-x})_5(PO_4)_3OH]$ at 25°C, J. Chem. 2017 (2017) 4619159, https://doi.org/10.1155/2017/4619159.
[41] M.M.J. van Rijt, S.W. Nooteboom, A. van der Weijden, W.L. Noorduin, G. de With, Stability-limited ion-exchange of calcium with zinc in biomimetic hydroxyapatite, Mater. Des. 207 (2021), https://doi.org/10.1016/j.matdes.2021.109846 109846.
[42] R.D. Shannon, Revised effective ionic radii and systematic studies of interatomic distances in halides and chalcogenides, Acta Crystallogr. Sect. A. 32 (5) (1976) 751–767, https://doi.org/10.1107/S0567739476001551.
[43] D.A. McKeown, I.S. Muller, A.C. Buechele, I.L. Pegg, Local environment of Zn in zirconium borosilicate glasses determined by X-ray absorption spectroscopy, J. Non. Cryst. Solids. 261 (1-3) (2000) 155–162, https://doi.org/10.1016/S0022-3093(99)00588-8.
[44] J.A. Biscardi, E. Iglesia, Reaction pathways and rate-determining steps in reactions of alkanes on H-ZSM5 and Zn/H-ZSM5 catalysts, J. Catal. 182 (1) (1999) 117–128, https://doi.org/10.1006/jcat.1998.2312.
[45] Y. Tang, H.F. Chappell, M.T. Dove, R.J. Reeder, Y.J. Lee, Zinc incorporation into hydroxylapatite, Biomaterials 30 (15) (2009) 2864–2872, https://doi.org/10.1016/j.biomaterials.2009.01.043.
[46] T. Takatsuka, J. Hirano, H. Matsumoto, T. Honma, X-Ray absorption fine structure analysis of the local environment of zinc in dentine treated with zinc compounds, Eur. J. Oral Sci. 113 (2) (2005) 180–183, https://doi.org/10.1111/j.1600-0722.2005.00194.x.
[47] B. Ravel, S.D. Kelly, The difficult chore of measuring coordination by EXAFS, AIP Conf. Proc. 882 (2007) 150–152, https://doi.org/10.1063/1.2644458.
[48] A.D. Wilson, S. Crisp, Ionomer cements, Br. Polym. J. 7 (5) (1975) 279–296, https://doi.org/10.1002/pi.4980070502.
[49] S.G. Griffin, R.G. Hill, Influence of glass composition on the properties of glass polyalkenoate cements. Part I: Influence of aluminium to silicon ratio, Biomaterials 20 (1999) 1579–1586, https://doi.org/10.1016/S0142-9612(99)00058-7.
[50] L.M. Gordon, L. Tran, D. Joester, Atom probe tomography of apatites and bone-type mineralized tissues, ACS Nano 6 (12) (2012) 10667–10675, https://doi.org/10.1021/nn3049957.
[51] F.J.G. Cuisinier, P. Steuer, J.-C. Voegel, F. Apfelbaum, I. Mayer, Structural analyses of carbonate-containing apatite samples related to mineralized tissues, J. Mater. Sci. Mater. Med. 6 (2) (1995) 85–89, https://doi.org/10.1007/BF00120413.
[52] I. Mayer, J.D.B. Featherstone, Dissolution studies of Zn-containing carbonated hydroxyapatites, J. Cryst. Growth. 219 (1-2) (2000) 98–101, https://doi.org/10.1016/S0022-0248(00)00608-4.
[53] S. Bentov, B.A. Palmer, B. Bar-On, Y. Shelef, E.D. Aflalo, A. Sagi, Reinforcement of bio-apatite by zinc substitution in the incisor tooth of a prawn, Acta Biomater. 120 (2021) 116–123, https://doi.org/10.1016/j.actbio.2020.07.039.